Supporting Information for

Micro-fabricated ultra-rapid desalting device for nano-electrospray ionization mass spectrometry

Ivan A. Tibavinsky,[a] Peter A. Kottke[a] and Andrei G. Fedorov*[a,b]

[a] George W. Woodruff School of Mechanical Engineering and [b] Parker H. Petit Institute for Bioengineering & Biosciences, Georgia Institute of Technology, Atlanta, GA 30332

*E-mail: agf@gatech.edu ; Address: Georgia Institute of Technology, School of Mechanical Engineering, 771 Ferst Dr NW, Atlanta, GA 30332; Tel: (404) 385-1356

The supporting information includes

1) details of the microfabrication process, including process flow diagrams, process parameters, descriptions of a custom wafer holder used for rapid aluminum deposition, and characterization of the porous alumina

2) description of the device package, including fluidic connections and sealing

3) description of the titration procedure used to characterize dialysis effectiveness

4) description of the model used for simulation of the device, including the Matlab code

5) description of the experimental determination of membrane hydraulic resistance.

MICRO-FABRICATION DETAILS

("Steps" refer to Fig. S-1)

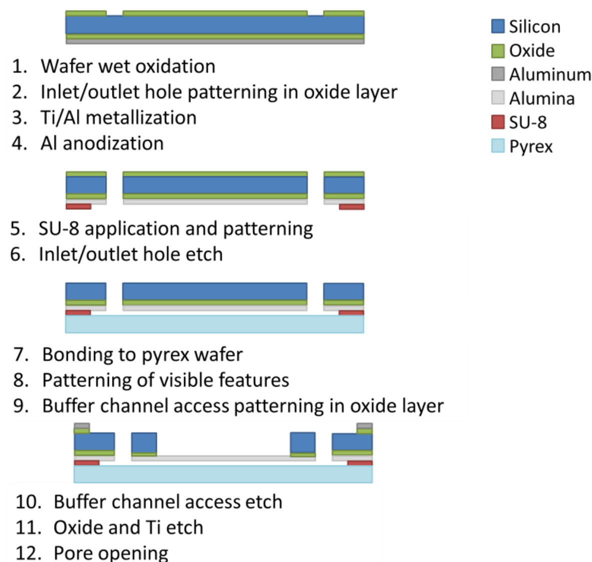

Figure S-1 Device micro-fabrication process flow diagram.

First, a double side polished 4 inch silicon wafer of (100) orientation was dipped in basic piranha at 120°C for 10 minutes (CMOS Cleaning Station), and subsequently spin dried with standard parameters (CMOS Spin Rinse Drier). Then, a 3 µm thick layer of oxide was thermally grown by wet oxidation at 1100°C for 18 hours (Tystar Poly Furnace) (Step 1). In order to define the inlet and outlet holes, which had a diameter of 60 µm, photolithography was then performed. Shipley's SPR 220 photoresist was spin-coated (250 rpm, 1000 rpm/s, 5s followed by 2000 rpm, 500 rpm/s,40 s) (BLE Spinner), and the wafer was baked at 110°C for 3 minutes. Then, the substrate was exposed to 500 mJ/cm^2 of 405 nm UV radiation (TSA Mask Aligner), and subsequently developed for 4 minutes in MF-319. After rinsing with deionized (DI) water, the photoresist within 5 mm from the edge of the wafer was removed with a swab dipped in acetone so that the substrate would not stick to the clamp of the Plasma-Therm ICP. Then, the wafer was hard baked at 100°C for 15 minutes. This resulted in a 9 µm thick layer of photoresist.

Table S-1 Silicon oxide dry etch parameters.

Pressure	5 mtorr
Ar flow rate	5 sccm
C_4F_8 flow rate	15 sccm
CO_2 flow rate	28 sccm
ICP power	800 W
Chuck power	40 W
Time	35 min

The pattern in the resist was then transferred onto the oxide layer by Inductively Coupled Plasma (ICP) etch with the parameters outlined on Table S-1 (Plamsa-Therm ICP), and the photoresist was then stripped by rinsing it with AMI (acetone, methanol, and isopropyl alcohol) in that order. (Step 2).

Following the inlet and outlet hole patterning on the oxide layer, the wafer was cleaned in 3:1 acid piranha for 15 minutes with no additional heat to the one produced by the exothermic reaction of the mixture. Then, a metallization of a titanium adhesion layer followed by an aluminum layer was performed by e-beam evaporation (CHA E-beam).

Differences in pressure on either side of the alumina membrane during experimental testing of the MD device require the membrane to be several microns thick in order to maintain mechanical stability. Since typical microfabrication metallization techniques result in maximum thicknesses of hundreds of nanometers, the setup in the chamber of a CHA E-beam evaporation system was modified as shown in Fig. S-2. Four clamps were attached to the standard holder and a custom

holder was attached to them with chains. As Figure Fig. S-3 illustrates, up to four 100 mm silicon wafers could be attached to the custom holder with Kapton tape. A 50 mm hole in the middle allowed material to be deposited on the crystal sensor of the tool, which was necessary to monitor and control metallization conditions during the process. In this manner, the substrates were suspended 30 cm away the source, which resulted in a deposition rate close to twice as high than if the standard holder had been used. As a result, the metal layers deposited were significantly thicker than measured by the sensor of the tool, but the thickness uniformity across the wafer was significantly affected. The actual total thickness of both layers decreased along the diameter of the wafer from 7.2 μm at the flat to 4.4 μm at the opposite side. The final thickness and deposition rate of the titanium layer as measured by the sensor were 25 nm, and 1 Å/s respectively, and those of the aluminum layer were 2.5 μm, and 5 Å/s also as measured by the sensor (Step 3).

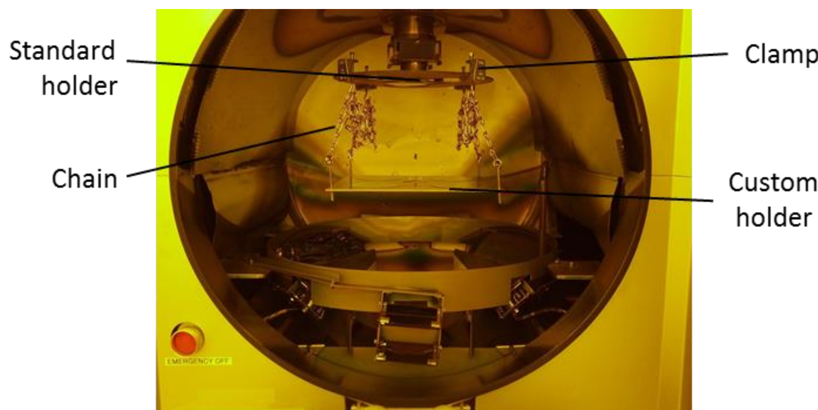

Figure S-2 E-beam evaporation chamber during deposition of alumina precursor material.

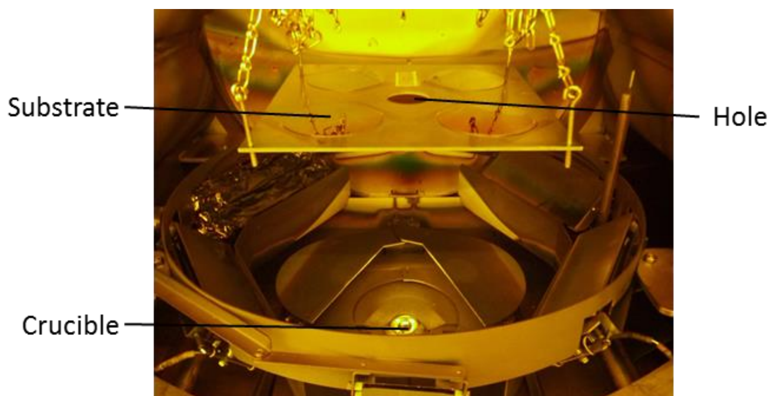

Figure S-3 Custom substrate holder during deposition of alumina precursor material.

In order to fabricate the porous membranes, the aluminum was then anodized for 30 minutes in 2 L of 0.3 M oxalic acid at 0°C in a jacketed beaker cooled by a recirculating ethylene glycol solution maintained at -1 °C by a chiller. A potential of 40 V with respect to a graphite rod 30 cm in length and 3 mm in diameter was applied. The thin layer of alumina created during this step was then stripped by dipping the wafers in 1.5% chromic acid and 5% phosphoric acid at 65°C in order to expose the organized preferred nucleation points for the next anodization, which was performed with the same parameters as the first one for 6 hours to ensure complete anodization of the aluminum (Step 4). This process results in a structured material that consists of parallel cylindrical pores of length equal to the thickness of the alumina. A Scanning Electron Microscope (SEM) micrograph and a tapping mode atomic force microscope (AFM) scan of the surface are shown in Fig. S-4. The pores are approximately 50 nm in diameter. The porosity was determined using the manipulated micrograph in Fig. S-5. By calculating the ratio of black pixels to white pixels in the image, the proportion of pores-to-inactive area can be calculated. Since the pores are known to be parallel, the volume proportion was assumed to be equal. In this manner, it was determined that the pores comprise close to 25% of the membrane total volume.

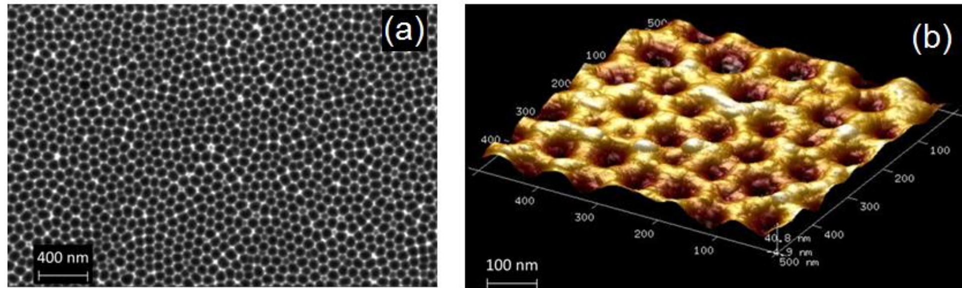

Figure S-4 (a) SEM micrograph and (b) AFM tapping mode scan of alumina membrane.

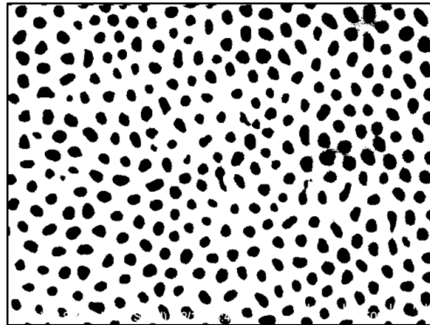

Figure S-5 Manipulated alumina membrane micrograph used for porosity determination.

Following the creation of the alumina membrane, the wafer was squirted for at least five seconds with each of the AMI solvents. Then, a 6.5 µm layer of SU-8 3005 was spin-coated (250 rpm, 1000 rpm/s, 5s followed by 2000 rpm, 500 rpm/s,40 s) (BLE Spinner) on to the porous alumina side of the wafer, and subsequently, the substrate was baked at 95°C for 2 minutes and 30 seconds. Channels were patterned with backside alignment to pair up the ends of the channels to their inlets and outlets. The substrate was exposed to 225 mJ/cm^2 of 365 nm UV light (EVG Mask Aligner) and post-exposure baked at 95°C for 2 minutes and 30 seconds once again. Then, the resist was developed in SU-8 developer for 2 minutes, and subsequently rinsed with IPA only (Step 5). After this step and until bonding to a Pyrex substrate was performed, the wafer was not rinsed with any fluids other than IPA and care was taken to not expose the substrate to white light by covering it with aluminum foil whenever transportation out of a yellow light area was required.

The area within 5 mm from the border of the wafer was then lightly covered with cool grease on the side that had patterned SU-8 using a swab. A carrier wafer, which had 1 µm layer of silicon oxide, was firmly pushed against the wafer on the same side. In this manner, the two substrates were attached to each other for ICP etch of silicon. The carrier wafer and the cool grease also served to protect the SU-8 from white light. On the side of the processed wafer that was still accessible, the perimeter of the wafer was covered with Kapton tape to protect the areas from which oxide was unwantedly removed due to the removal of photoresist on the edges before performing Step 2. Alignment marks were also protected in the same way. The inlet and outlet sample channel holes were subsequently etched with 800 cycles of a Bosch process with the parameters outlined in Table S-II (STS ICP). After ensuring complete etch of the silicon by observing light through the holes, the tape on the borders and on the alignment marks was removed.

In order to remove the remaining membranes of oxide, titanium, and alumina at the bottom of the inlet and outlet holes, droplets of a 1 M solution of sodium hydroxide were carefully placed on the alumina side of the holes by pressing with a swab dipped in the solution to ensure that the fluid would make contact with the alumina. After 5 minutes, the droplets were carefully removed with a fresh swab, and then, the wafer was sonicated in an IPA bath for 10 minutes (Step 6). Complete opening of the holes was ensured by softly pushing the wafer against a hard surface coated with IPA. As expected, IPA visibly flowed through the holes.

Following the inlet/outlet hole opening, the substrate was bonded to a Pyrex wafer applying a pressure of 10 bar at a temperature of 130°C for 30 minutes (Step 7) (Obducat Nanoimprinter).

Table S-2 Silicon etch parameters.

	Passivation	Etch
SF_6 flow rate	0	130 sccm
C_4F_8 flow rate	85 sccm	0
Coil Power	800 W	800 W
Platen Power	0 W	10 W
Pressure	0.1 mTorr	0.1 mTorr
Time	9 s	11 s

Visible features such as dicing lines were necessary in order to handle the devices and align them in the package when finished. These were made by patterning SPR 220 with the previous parameters on the side of the bonded substrate that had the inlet and outlet sample holes. Then, a layer of 25 nm of titanium followed by a 100 nm layer of aluminum was deposited by e-beam (CHA E-beam) on the patterned photoresist at the standard distance from the source, and then lift off was performed (Step 8).

Following the patterning of visible features, once again, SPR 220 was applied and patterned with the previous recipe on the side of the substrate that had the sample holes. This time, in addition to removing the photoresist close to the border of the wafer, care was taken to remove glue left over from the Kapton tape applied before Step 6 in order to avoid the sample sticking to the Plasma-Therm ICP. Buffer access to the membranes was patterned on the oxide with the ICP etch described in Table S-I (Step 9) (Plasma-Therm ICP). Leaving the photoresist that served as a mask to pattern the silicon oxide on the wafer, silicon was etched with 600 cycles of the ICP etch outlined in Table S-2 (Step 10)(STS ICP). Since the photoresist was the mask for the etching of these bigger features, it was not necessary to cover the borders with Kapton tape once again.

In order to remove the oxide and the titanium on the resulting alumina membranes, the photoresist on the borders of the wafer was removed, as before, and ICP etch was once again used with the parameters in Table S-1 (Step 11) (Plasma-Therm ICP). Finally, the pores in the membranes were opened on the backside by dipping the wafer in 5% phosphoric acid at room temperature for 45 minutes (Step 12). The fabrication process ends by soaking the devices in acetone for 2 days to dissolve any lose photoresist and prevent clogs.

PACKAGE

The purpose of the package, which is depicted in Fig. S-6, is to provide fluidic connections for the sample inlet, buffer inlet and buffer outlet, to define the buffer flow path, and to provide for sample collection. The package consists of two pieces of transparent polycarbonate 0.5 inches thick. The bottom piece is only used to transmit clamping force. A gasket defines the buffer flow path. The gasket groove was machined 0.5 mm in both depth and width, and a 1 mm thick laser cut silicone gasket of 30A hardness was inserted, as shown in Fig. S-6(b). The sample channel inlet and outlet are sealed to the fluidic ports using AS568-002 Buna-n O-rings in O-ring glands machined in the package. Fluidic ports are machined to accept 1/4-28 thread flat bottom nuts per manufacturer's specifications (Idex Scientific P-202 and P-200).

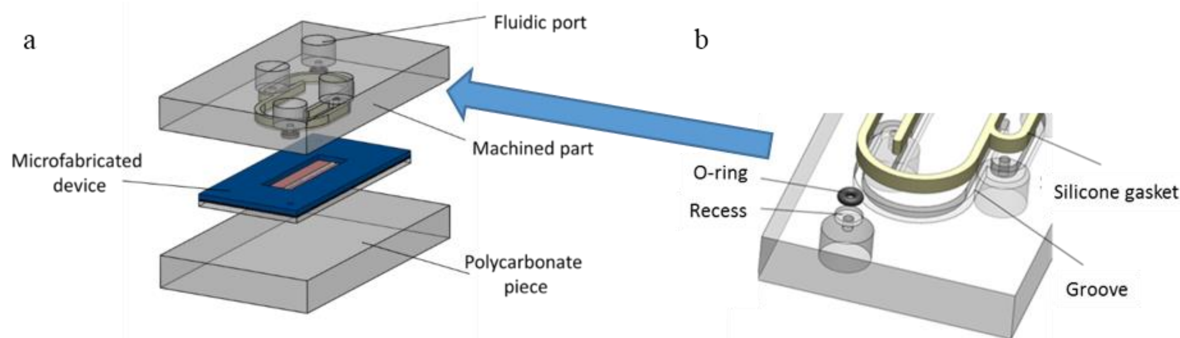

Figure S-6 Package details: (a) depicts assembly of micro-fabricated device between package components, and (b) shows sealing components on the top of the two polycarbonate parts in (a)– a gasket and o-rings in machined grooves. The two pieces of polycarbonate are clamped together with screws that are not shown to improve the clarity of the pictures.

CHARACTERIZATION

The effectiveness of a device microfabricated and packaged as described above at removing salt was tested by forcing a salt solution through the sample channel and deionized water through the buffer channel. The salt solution was collected at the sample outlet, and its concentration was measured. By assessing the change in salt concentration in the solution after treatment with the system, the effectiveness of the device was determined. Fig. 4 shows the schematic of the experimental setup used for these experiments.

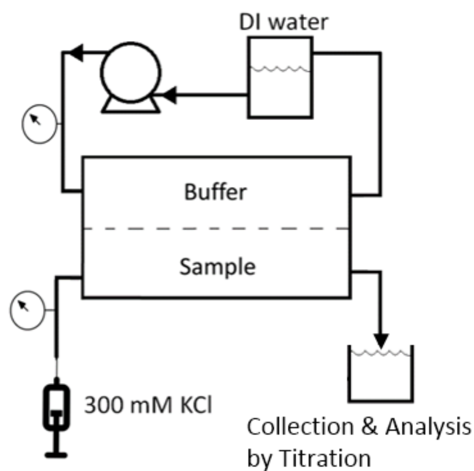

Figure S-7 Schematic of micro-fabricated salt removal device characterization experiment.

DI water from a 1 L reservoir is pumped through the buffer channel with a peristaltic pump (Watson-Marlow 205U) running at 50 rpm with a 0.025” bore tube (Watson-Marlow 982.0063.000), thus generating a flow rate of 50 ml/hr. The pressure in the line between the pump and the device is monitored with a microfluidic pressure transducer (LabSmith uPS0800-T116). In the sample channel, a 300 mM solution of KCl in DI water is introduced with a syringe pump (KD Scientific 100) at flow rates ranging from 30 to 150 µl/hr. The pressure in the sample inlet line is also monitored (LabSmith uPS0800-C360). The sample is collected at the outlet well, which is covered during each experimental run to prevent the solvent in the sample from evaporating. Chloride concentration of the collected sample is measured using argentometric titration (Mohr method).[24] Specifically, 30 µl of dialyzed sample are added to a 2 ml cuvette in which 250 µl of a commercial solution of potassium chromate (Hach 1057-66) has been diluted in 500 µl of DI water. In parallel, 1 ml of 300 mM potassium chloride is added to a second cuvette in which the same mixture of indicator and water has been prepared. A small amount of titrant is added to this second cuvette to produce the turbid yellow color that characterizes the solution before the endpoint is reached. A digital titrator (Hach 1690001) is used to dispense small measured amounts of 0.025 N silver nitrate to the cuvette to which the sample to be measured was added, and the color of this solution is compared to that of the second cuvette to facilitate consistent and accurate determination of the titration endpoint.

MODEL

To facilitate analysis and understanding of the desalting quantification experimental results, and to serve as a tool for future device design and operational guidance, we have developed a simple model that captures all relevant dominant physics of the micro-fabricated desalting device. The two dimensional steady state model is based on the following assumptions and simplifications: (1) pressure drop in the sample channel can be well approximated using a uni-directional (parallel) laminar fully developed flow model in spite of the existence of trans-membrane flow; (2) salt concentration in the buffer solution far from them membrane is approximately zero; (3) mass transfer of the salt can be well described using a Fickian diffusion model with an effective binary diffusion coefficient; (4) properties (e.g., density, viscosity) of the sample liquid are uniform; and, (5) transmembrane flowrates are low enough that the Peclet number for mass transfer remains small in the membrane and mass transfer across the membrane is dominated by diffusion while (6) sample channel flowrates remain sufficiently large that the mass transport in the sample flow direction is dominated by advection, i.e., the Peclet number for mass transfer remains large in the sample channel. Figure S-8 is a schematic depicting the geometry, control volume and nomenclature used for the model.

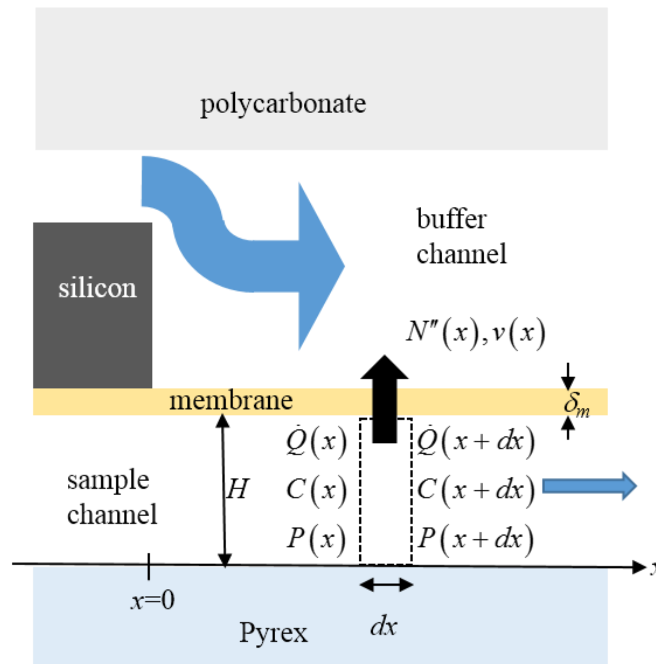

Figure S-8 Schematic of differential control volume in the sample used to develop the model of the desalting device. Salt molar concentration, C, changes due advection/diffusion from the bulk in the sample to the membrane internal surface, diffusion through the membrane of thickness, δ_m, and advection/ diffusion into the buffer. Sample volumetric flow rate, $\dot{Q}$, is changed by the local pressure difference (sample-to-buffer) driven transmembrane mean velocity, v, and the pressure in the sample stream, P, decreases in the flow direction. The blue arrows indicate the flow direction, and are aligned with increasing position coordinate, x. The solution domain is between x=0, which is the point in the flow-wise direction at which the membrane top is first exposed to the buffer stream, and x=L, where L is the total length of the section of the sample channel in which salt removal occurs. The sample channel has width, w, and height, H.

Using the control volume depicted in Fig. 5, and the assumptions stated above, mass conservation applied to the solution in a sample channel of width w dictates that the volumetric flow obey the following first order ODE

$$\frac{d\dot{Q}}{dx} = -wv \qquad \text{(S-1)}$$

Eq. (S-1) requires an inlet condition, which is simply obtained by requiring the volumetric flow rate of solution at the beginning of the active (*i.e.*, where diffusion across the membrane occurs) section of the sample channel to equal the flow rate provided by the syringe pump, $\dot{Q}_0$, *i.e.*, $\dot{Q}(x=0) = \dot{Q}_0$. Mass conservation applied to the species whose removal is being considered is expressed via a first order ODE for species concentration:

$$\frac{dC}{dx} = -\frac{1}{\dot{Q}}\left(wN'' + C\frac{d\dot{Q}}{dx}\right) \quad \text{(S-2)}$$

where N'' is the molar flux leaving the control volume through the membrane, and the inlet condition imposes the introduced concentration, C_0, at x=0: $C(x=0)=C_0$. The local pressure is obtained through application of momentum conservation simplified via assumption (1) so that the pressure gradient is found assuming a Poisseuille flow:

$$\frac{dP}{dx} = -\frac{12\mu\dot{Q}}{wH^2} \quad \text{(S-3)}$$

where μ is the liquid dynamic viscosity, and Eq. (S-3) has an inlet condition imposing a specified pressure , P_0, at x=0: $P(x=0)=P_0$. The model expressed in Eqs. (S-1)-(S-3) and initial conditions, requires equations describing the local transmembrane molar flux N'' and the transmembrane local mean velocity, v, both of which vary in the flow direction, *i.e.*, are functions of position, x. The molar flux is equal to the concentration difference between the sample and buffer channels divided by the net resistance to mass transfer, which is the sum of the resistance in the sample channel, across the membrane, and in the buffer:

$$N''(x) = \frac{C(x)}{1/h_s + \delta_m/(\phi D) + 1/h_b} \quad \text{(S-4)}$$

where D is the effective binary diffusion coefficient, ϕ is the membrane porosity, h_s and h_b are the local convective mass transfer coefficients in the sample and the buffer, respectively, and the concentration in the buffer is negligibly small. The convective mass transfer coefficient in the sample channel is assumed constant and is given by [25]

$$h_s = 2.5\frac{D}{H} \quad \text{(S-5)}$$

which is valid for fully developed flow, while the non-standard geometry for the buffer channel requires that the convective mass transfer coefficient there be determined by numerical simulation (see supporting online information). The transmembrane velocity, v, is found by using the permeability, κ, of the membrane, which is experimentally measured (see supporting online information), and the driving pressure difference between the sample and buffer flows:

$$v = \kappa(P - P_b) \quad \text{(S-6)}$$

where P_b is the pressure in the buffer channel, which is essentially atmospheric pressure for the flow rates and buffer channel configurations used in this work. The system of equations that comprise the model, Eqs. (S-1)-(S-6), supplemented by the buffer mass transfer coefficient determined by simulation, are solved numerically using MATLAB (method details and program code are provided as online supplemental information).

BUFFER MASS TRANSFER COEFFICIENT DETERMINATION USING COMSOL

Due to the geometry that resulted from the packaging of the device, as is shown in Fig. S-9, a computational approach was necessary to calculate the mass transfer coefficient.

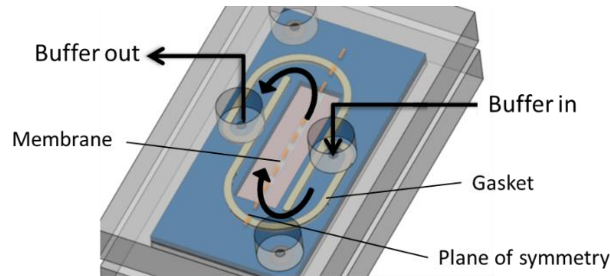

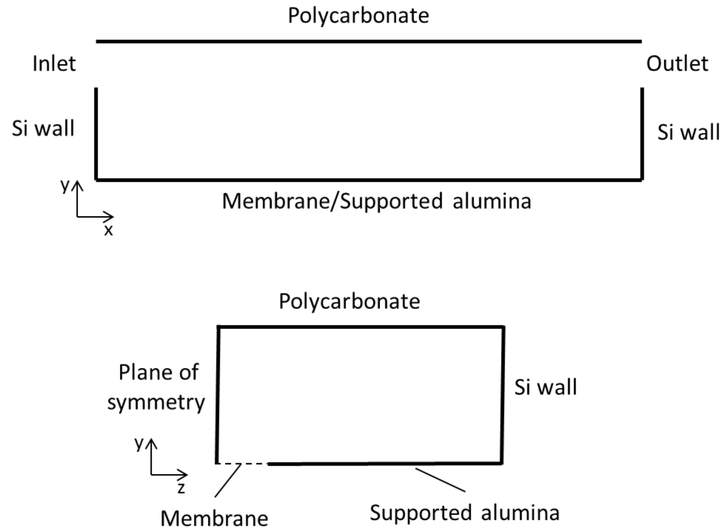

Figure S-9 Buffer fluid flow path.

Figure S-10 shows two cross sections of the three-dimensional domain in which the governing equations for mass transfer and fluid flow, Equations (S-7) to (S-9), were discretized and solved simultaneously using COMSOL. The figure also illustrates what every one of the surfaces is equivalent to in the physical device. All the dimensions were the same as they were in the final assembly. A plane of symmetry was implemented along the center of the membrane in order to reduce the domain size and optimize computational resources. Figure S-9 shows were this plane is located in the experimental arrangement.

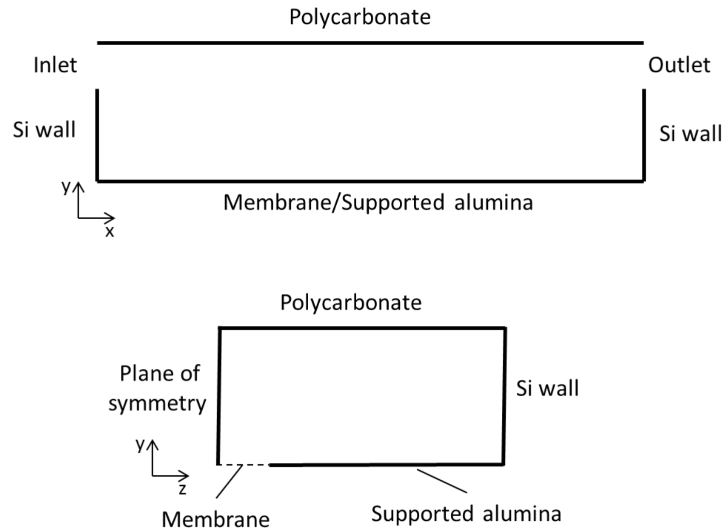

Figure S-10 Computational simulation domain.

$$\nabla \cdot \left(-D_i \nabla C_b\right) + \vec{U} \cdot \nabla C_b = 0 \tag{S-7}$$

$$\rho\left(\vec{U} \cdot \nabla\right)\vec{U} = -\nabla P_b + \mu \nabla^2 \vec{U} \tag{S-8}$$

$$\nabla \cdot \vec{U} = 0 \tag{S-9}$$

In Equations (S-7) to (S-9), $\vec{U}$ is the velocity vector, D_i is the diffusion coefficient of potassium chloride in water, and ρ is the density of the fluid. Table S-3 summarizes the boundary conditions imposed on each of the surfaces based on how they were believed to behave in the physical system. A constant normal inflow velocity with no species concentration was imposed at the inlet. The fluid velocity on this surface was calculated from the known cross sectional area of the inlet and

the flow rate used during experiments. At the outlet, a pressure of 0 was assigned, while diffusive transport was ignored. At the symmetry plane no normal fluid velocity and no mass flux were imposed. Since mass transfer boundary conditions at the membrane are not trivial to determine based on the experimental setup, two different scenarios were considered. No-slip condition with a constant concentration, and with a constant mass flux were studied. In the table $\vec{n}$ is the vector normal to the surface.

Table S-3 Computational model boundary conditions.

Surface	Mass Transfer Boundary Condition	Fluid Flow Boundary Condition
Inlet	$C_b = 0$	$\vec{U} = -0.07\,\vec{n}$ (m/s)
Outlet	$-\vec{n}\cdot(D_i\nabla C_b) = 0$	$P_b = 0$
Membrane	$C_b = 300$ (mol/m^3)	$\vec{U} = 0$
	$-\vec{n}\cdot\left(D_i\nabla C_b + \vec{U}C\right) = 0.01$ (mol/m^{2}s)	$\vec{U} = 0$
Plane of symmetry	$-\vec{n}\cdot\left(D_i\nabla C + \vec{U}C\right) = 0$	$\vec{U}\cdot\vec{n} = 0$
All other surfaces	$-\vec{n}\cdot\left(D_i\nabla C + \vec{U}C\right) = 0$	$\vec{U} = 0$

The local mass transfer coefficient h_b was calculated using $h_b = -N''/\left(C_b - C_\infty\right)$ where N'' is the local molar flux normal to the membrane, C_b is the concentration at the membrane surface, and C_∞=0, and averaged over the width of the membrane. The results are plotted along with the two dimensional velocity profile at the symmetry plane in Fig. S-11. The plot shows that throughout the length of the computational domain the mass transfer coefficient is changing. Close to the silicon walls located below the inlet and outlets, a small mass transfer coefficient results from the stagnation of fluid close to the membrane caused by the sudden change in channel geometry. The MATLAB code (see below) was implemented using both local values of the buffer mass transfer coefficient h_b and a single average value of 2.78E-5 m/s. The impact on predicted salt removal efficiency was less than 1%.

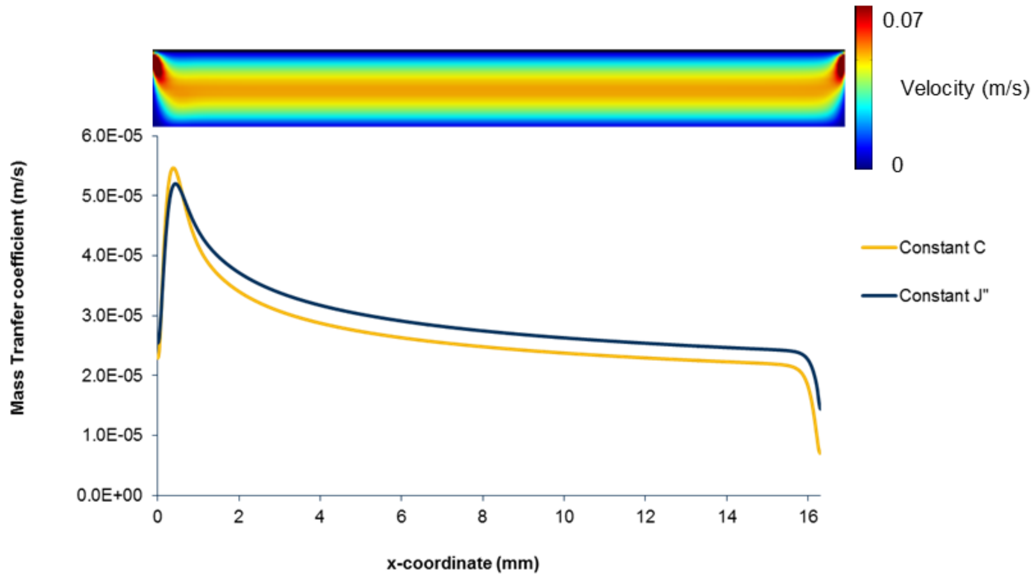

Figure S-11 Mass transfer coefficient and velocity field.

MATLAB Code

```
function DialysisEfficiency
% Initialization
L=163500E-6; %Length of the sample channel [m]
H=6.5E-6;   %Height of the sample channel [m]
Q_i=8.33E-12; %Sample flow rate enterring sample channel, [m^3/s], 8.33E-12m^3/s= 30
[ul/hr]
w=100E-6; %Width of the sample channel [m]
kappa = 1.15E-11; %membrane hydraulic permeability [m/(Pa*s)]measured experimentally
D_i=2e-9; %Diffusion coefficient for chloride in water m^2/s 2E-9,
%For protein use equation of Young et al D_i=8.34E-12*T/eta/Mw^(1/3)
C_i=300; %initial concentration for chlroide mol/m^3
t_m=5E-6; %alumina membrane thickness
P_m=.2528; %membrane porosity determined via SEM micrograph
P_b=0; %buffer pressure (gage)
mu_w=1.002E-3; %Dynamic viscosity of solvent [Pa*s]
P_i=57000; %Inlet pressure (gage) [Pa]
Sh_s=2.5; %Sample Sherwood number
h_s=Sh_s*D_i/H;
h_b=2.78E-5; %Buffer mean mass transfer coefficienct determined numerically [m/s]
x_span=[0 L];
init=[C_i;Q_i;P_i;0];
sol=ode45(@dvdx,x_span,init);
C_o =sol.y(1,end)
Q_o =sol.y(2,end)
eff_C =100*(1-C_o /C_i)
t_res =sol.y(4,end)
%_______________________________________________________________________
    function dvecdx = dvdx(x,y)
        C=y(1);
        Q=y(2);
        P=y(3);
        J=C/(1/h_s+(t_m/(D_i*P_m))+1/h_b);
        dQdx=-kappa*w*(P-P_b);
        dCdx=-J*w/Q-C/Q*dQdx;
        dPdx=-12*mu_w*Q/w/H^3;
        dtdx=w*H/Q;
        dvecdx=[dCdx;dQdx;dPdx;dtdx];
    end
%_________________________________________________________________________
end
```

MEMBRANE HYDRAULIC RESISTANCE MEASUREMENT

The transmembrane velocity, v, is found by using the permeability, κ, of the membrane, which is experimentally measured using the experiment depicted in Fig S-12: $\kappa = Q_{cross} / (A_m \Delta P)$ where Q_{cross} is the flow rate across the membrane caused by an uniform pressure difference between the two channels, ΔP, and A_m is the total membrane area.

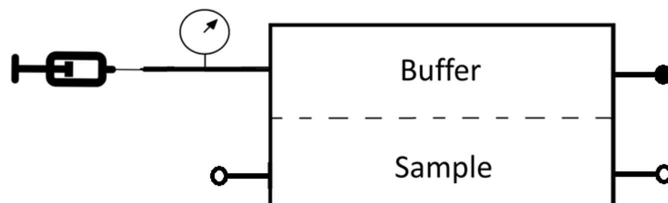

Figure S-12 Experimental setup for membrane hydraulic resistance characterization.

A 1 ml syringe containing DI water was connected to the inlet of the buffer channel, and the outlet was closed. Both, the inlet and the outlet of the sample channel were left open, and the entire channel was assumed to remain at ambient pressure. The pressure in the line from the syringe to the buffer inlet, which was assumed to be the same as in the entire buffer chamber, was constantly monitored with a microfluidics pressure transducer (LabSmith uPS0800-T116) as a constant force was applied to the syringe. This line consisted of PEEK tubing, which has a low elastic yield.

To calculate κ, Q_{cross} is the change in volume observed in the syringe over the duration of the experiment, 120 μL , divided by the time over which the force was applied, 10270 seconds, and the membrane area, A_m is 1.635E-6 m^2 from the device geometry. ΔP was 619 kPa, the average value of the constantly monitored pressure, which is plotted in Fig. S-13 as a function of time. This resulted in a κ value of 1.15E-11 m/s-Pa

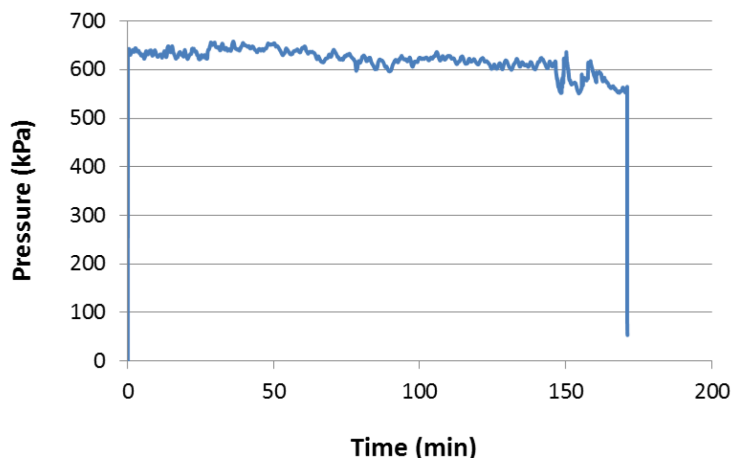

Figure S-13 Measured pressure at buffer inlet as a function of time.